NASA/TM—2013-217888/PART1

Low Temperature Creep of Hot-Extruded Near-Stoichiometric NiTi Shape Memory Alloy

Part I: Isothermal Creep

S.V. Raj and R.D. Noebe
Glenn Research Center, Cleveland, Ohio

June 2013

NASA STI Program . . . in Profile

Since its founding, NASA has been dedicated to the advancement of aeronautics and space science. The NASA Scientific and Technical Information (STI) program plays a key part in helping NASA maintain this important role.

The NASA STI Program operates under the auspices of the Agency Chief Information Officer. It collects, organizes, provides for archiving, and disseminates NASA's STI. The NASA STI program provides access to the NASA Aeronautics and Space Database and its public interface, the NASA Technical Reports Server, thus providing one of the largest collections of aeronautical and space science STI in the world. Results are published in both non-NASA channels and by NASA in the NASA STI Report Series, which includes the following report types:

- TECHNICAL PUBLICATION. Reports of completed research or a major significant phase of research that present the results of NASA programs and include extensive data or theoretical analysis. Includes compilations of significant scientific and technical data and information deemed to be of continuing reference value. NASA counterpart of peer-reviewed formal professional papers but has less stringent limitations on manuscript length and extent of graphic presentations.

- TECHNICAL MEMORANDUM. Scientific and technical findings that are preliminary or of specialized interest, e.g., quick release reports, working papers, and bibliographies that contain minimal annotation. Does not contain extensive analysis.

- CONTRACTOR REPORT. Scientific and technical findings by NASA-sponsored contractors and grantees.

- CONFERENCE PUBLICATION. Collected papers from scientific and technical conferences, symposia, seminars, or other meetings sponsored or cosponsored by NASA.

- SPECIAL PUBLICATION. Scientific, technical, or historical information from NASA programs, projects, and missions, often concerned with subjects having substantial public interest.

- TECHNICAL TRANSLATION. English-language translations of foreign scientific and technical material pertinent to NASA's mission.

Specialized services also include creating custom thesauri, building customized databases, organizing and publishing research results.

For more information about the NASA STI program, see the following:

- Access the NASA STI program home page at *http://www.sti.nasa.gov*

- E-mail your question to *help@sti.nasa.gov*

- Fax your question to the NASA STI Information Desk at 443–757–5803

- Phone the NASA STI Information Desk at 443–757–5802

- Write to:
  STI Information Desk
  NASA Center for AeroSpace Information
  7115 Standard Drive
  Hanover, MD 21076–1320

NASA/TM—2013-217888/PART1

Low Temperature Creep of Hot-Extruded Near-Stoichiometric NiTi Shape Memory Alloy

Part I: Isothermal Creep

S.V. Raj and R.D. Noebe
Glenn Research Center, Cleveland, Ohio

National Aeronautics and
Space Administration

Glenn Research Center
Cleveland, Ohio 44135

June 2013

Acknowledgments

The authors thank Mr. Darrell Gaydosh, Drs. Anita Garg, Bradley Lerch and Santo Padula for granting permission to cite or use their unpublished data. The authors also thank Prof. R. D. James, University of Minnesota, and Prof. P. Anderson, Ohio State University for discussions relating to some of the data included in this paper. Comments from Dr. Michael Nathal are greatly appreciated. This work was supported by the Subsonic Fixed Wing Project of NASA's Fundamental Aeronautics Program.

This work was sponsored by the Fundamental Aeronautics Program at the NASA Glenn Research Center.

Level of Review: This material has been technically reviewed by technical management.

Available from

NASA Center for Aerospace Information
7115 Standard Drive
Hanover, MD 21076–1320

National Technical Information Service
5301 Shawnee Road
Alexandria, VA 22312

Available electronically at http://www.sti.nasa.gov

Low Temperature Creep of Hot-Extruded Near-Stoichiometric NiTi Shape Memory Alloy
Part I: Isothermal Creep

S.V. Raj and R.D. Noebe
National Aeronautics and Space Administration
Glenn Research Center
Cleveland, Ohio 44135

Abstract

This two-part paper is the first published report on the long term, low temperature creep of hot-extruded near-stoichiometric NiTi. Constant load tensile creep tests were conducted on hot-extruded near-stoichiometric NiTi at 300, 373 and 473 K under initial applied stresses varying between 200 and 350 MPa as long as 15 months. These temperatures corresponded to the martensitic, two-phase and austenitic phase regions, respectively. Normal primary creep lasting several months was observed under all conditions indicating dislocation activity. Although steady-state creep was not observed under these conditions, the estimated creep rates varied between 10^{-10} and 10^{-9} s^{-1}. The creep behavior of the two phases showed significant differences. The martensitic phase exhibited a large strain on loading followed by a primary creep region accumulating a small amount of strain over a period of several months. The loading strain was attributed to the detwinning of the martensitic phase whereas the subsequent strain accumulation was attributed to dislocation glide-controlled creep. An "incubation period" was observed before the occurrence of detwinning. In contrast, the austenitic phase exhibited a relatively smaller loading strain followed by a primary creep region, where the creep strain continued to increase over several months. It is concluded that the creep of the austenitic phase occurs by a dislocation glide-controlled creep mechanism as well as by the nucleation and growth of deformation twins.

1.0 Introduction

Advanced aircraft (Ref. 1) and rotorcraft (Ref. 2) designs increasingly require an ability to move various parts of the vehicle to achieve certain design and performance objectives. For example, morphing aircraft with capabilities for real time, on-demand wing movements enable flexible design capabilities (Ref. 3). Similarly, aircraft equipped with chevron nozzles with an ability to move the chevrons in and out of the flow path of gases exhausting from the engines can reduce engine noise during take-off and landing while improving engine performance and efficiency during cruise (Refs. 4, 5, and 6). The incorporation of these advanced concepts in aircraft designs are expected to lower fuel consumption, reduce emissions, increase safety and diminish engine noise. The development of suitable actuator technologies is critical to enabling these adaptive structures.

The emphasis of current actuator technology development is increasingly dependent on the use of lightweight "smart materials" solid state technology (Ref. 7). Among them, shape memory alloy (SMA) actuators undergo a dimensional change due to the martensite (M) to austenite (A) transformation on heating. Since these dimensional changes can be large, SMA actuators are very suitable for applications requiring large displacements and a high work output (Ref. 6). There is a large body of evidence which suggests that thermal cycling of many of these SMAs under an applied stress results in an offset strain at the end of each cycle, where the start and end points of the hysteresis loop are displaced by a finite amount of strain (Ref. 6). This offset strain increases cumulatively during each subsequent thermal cycle, which is likely to decrease the effectiveness of the actuator in actual applications.

Since these thermal cycling tests are conducted under constant load conditions in the laboratory to simulate the actual operating conditions for the SMA actuators, the observance of these offset strains in binary and ternary NiTi alloys (Ref. 6) is intriguing. In this connection, some key questions arise:

a) Does near-stoichiometric NiTi exhibit significant creep in the temperature ranges between 300 and 473 K corresponding to the martensitic and austenitic phase fields, respectively?
b) What is the low temperature creep design stress limit for near-stoichiometric NiTi?
c) What are the creep characteristics of the austenitic and martensitic phases?
d) Is there any evidence of dislocation activity in these two phases?
e) What is the long-term stability of NiTi under constant stress under isothermal and thermal cycling conditions?

Determining answers to these questions is important for designing SMA actuators for long duration applications. Unfortunately, prior creep investigations on NiTi alloys were conducted above 743 K (0.47 T_m, where T_m is the absolute melting point) corresponding to the austenitic phase field and well outside the temperature range, where NiTi SMAs are likely to be used in aerospace applications (Refs. 8, 9, 10, 11, 12, 13, and 14). No prior creep data have been reported below 473 K (0.30 T_m) in either the austenitic or the martensitic phase fields. Additionally, there are no long term creep data on NiTi and it is difficult to assess the long term stability of these alloys for actuator applications if maintained under load for significant periods of time. The present investigation was undertaken to study the low temperature creep behavior of near-stoichiometric NiTi to seek answers to the above questions. The first part of the paper characterizes the isothermal creep of NiTi between 300 and 473 K, while the second part discusses the creep response of pre-crept NiTi when the temperature is cycled between 300 and 473 K under constant stress conditions.

2.0 Experimental Procedures

The single phase alloy used in this investigation had a nominal composition of Ni-45(wt.%)Ti approximately corresponding to the stoichiometric composition, Ni-50(at.%)Ti. Tensile specimens with threaded ends, and ridges precisely defining the gage section, were machined from hot-extruded rods (Figure 1). The grain size of the hot-extruded material varied between 20 and 60 μm (Ref. 15). The gage dimensions were measured using an optical traveling microscope, where five measurements were made along the gage length on each specimen. The average gage length was 20 ± 0.02 mm and the average gage diameter 3.2 ± 0.01 mm, where the errors represent 95 percent confidence values. Constant load tensile creep tests were conducted at absolute temperatures, T, of 300 (0.19 T_m), 373 (0.24 T_m) and 473 K (0.30 T_m) under applied initial stresses, σ, varying between 200 and 350 MPa using several constant load lever arm machines with lever arm ratios varying between 3:1 and 10:1. The specimen elongation was measured using extensometers attached to a pair of ridges machined on the specimen, where linear variable capacitance transducers measured the displacements of the extensometer heads. Three thermocouples were attached to the specimen to monitor the specimen temperature and the temperature gradient along the gage length. In order to ensure that the starting microstructures are similar in all the tests, all specimens were held at 523 K for 1 h before furnace cooling over a 20 to 25 h period to the test temperature under a low stress of 5 to 6 MPa. It should be noted that the starting microstructures of NiTi are expected to be martensitic, duplex and austenitic at 300, 373 and 473 K, respectively, at these low stresses (Ref. 16). The isothermal creep tests were conducted for up to about 15 months. Typically, each specimen was crept under a constant engineering stress for several hundred hours before conducting stress change tests. A few tests were also conducted on mild steel specimens to verify that the strain measurements were genuinely due to specimen elongation.

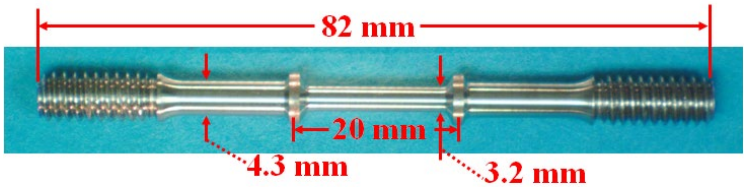

Figure 1.—Tensile creep specimen showing gage dimensions and general design.

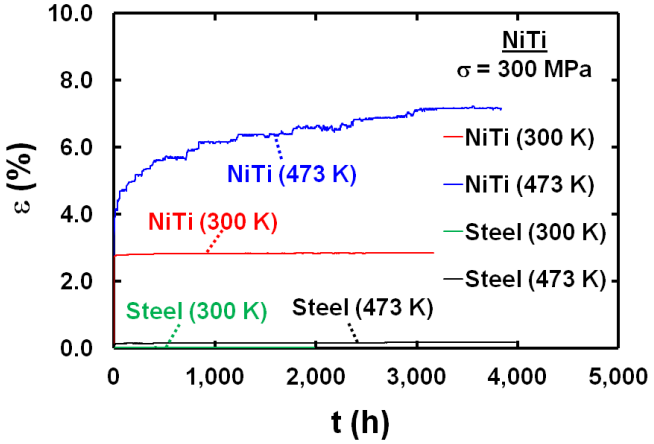

Figure 2.—Comparison of the creep strain, ε, versus time, t, plots for NiTi and mild steel at 300 and 473 K.

3.0 Results and Discussion

3.1 Comparison of the Creep Behavior of NiTi With Mild Steel

Figure 2 compares the creep curves plotted as true creep strain, ε, against time, t, for specimens tested at 300 and 473 K under an initial applied stress of 300 MPa. As noted earlier, the initial microstructures of the specimens prior to loading were martensitic and austenitic, respectively, at these temperatures and applied stress. The creep curves for the steel specimens tested at 300 and 473 K tested under 300 MPa are also shown in Figure 2 for comparison. The steel specimens exhibit a very small loading strain followed by logarithmic creep. In contrast, NiTi exhibits a relatively larger loading strain at 300 and 473 K followed by primary creep lasting several months with no discernable steady-state creep behavior. These observations suggest that the external factors did not significantly influence the strain measurements and represent genuine material behavior. The creep characteristics of NiTi at different temperatures will be discussed in the later sections.

3.2 Creep Limit

The creep limits at 300 and 473 K were determined by increasing the applied stress from an initial value of 200 MPa. In the case of the martensitic phase, the specimen was crept for 2035.6 h under an applied stress of 200 MPa before increasing the stress to 300 MPa; subsequently, the stress was periodically increased by about 5 percent of the previous stress. The specimen deformed in the austenitic range was initially crept for over 1000 h under an applied stress of 200 MPa followed by periodic stress increases of about 10 to 13 percent of the previous stress. In all cases, the specimen was crept for several hundred hours after each stress change.

Figure 3(a) and (b) show plots of ε versus time t, at 300 and 473 K, respectively, where the stress was periodically increased from 200 to 347.3 MPa. The broken lines depict the corresponding values of engineering stress; the temperature profile is also shown. The right hand axis gives the values of stress and temperature. Loading NiTi to 200 MPa at 300 K resulted in an increase in the creep strain to 0.46 percent followed by a small primary creep region, where the creep strain increased to about 0.53 percent in 2035.6 h corresponding to estimated creep rates, $\dot{\varepsilon}$, less than 1.3×10^{-10} s^{-1} approaching the resolution limits of measurements. A stress increase, $\Delta\sigma^{+}$, by 100 MPa to a new stress of 300 MPa resulted in a relatively large increase in strain by about 1.1 percent soon after the stress increase and further increased by an additional 0.41 percent in about 2000 h (Figure 4(a)). Interestingly, the variation in the creep strain, $\Delta\varepsilon^{+}$, with increasing time, Δt, after the stress increase exhibits a sigmoidal behavior for different values of $\Delta\sigma^{+}$.[1] The magnitude of $\Delta\varepsilon^{+}$ increases sharply with increasing Δt after an "incubation period" of gradually increasing $\Delta\varepsilon^{+}$ with increasing Δt. Significantly, the creep strain continued to increase more gradually for several weeks and months after the sharp increase in $\Delta\varepsilon^{+}$.

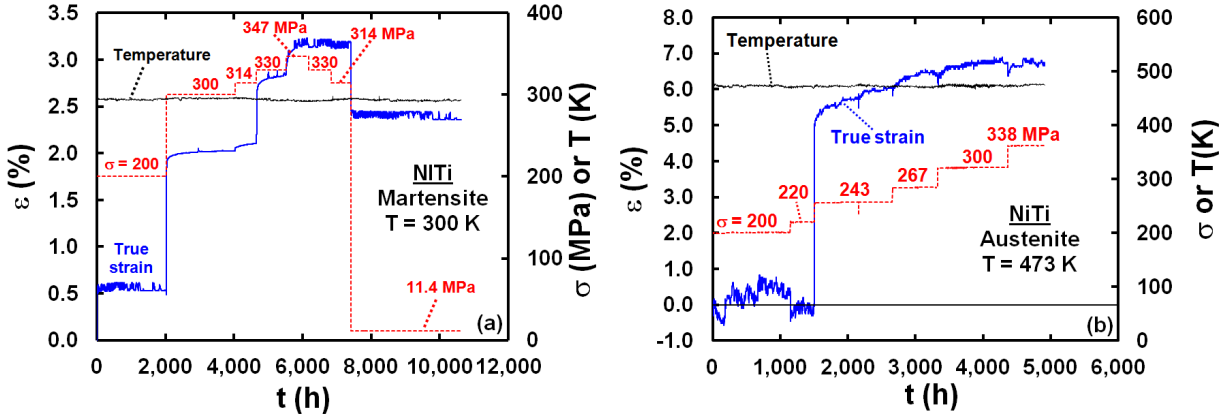

Figure 3.—Creep strain versus time plots for (a) NiTi martensite deformed at 300 K and (b) NiTi austenite deformed at 473 K showing the effect of stress changes on the nature of the creep curves. Insignificant creep was observed below 200 and 220 MPa for martensite and austenite, respectively.

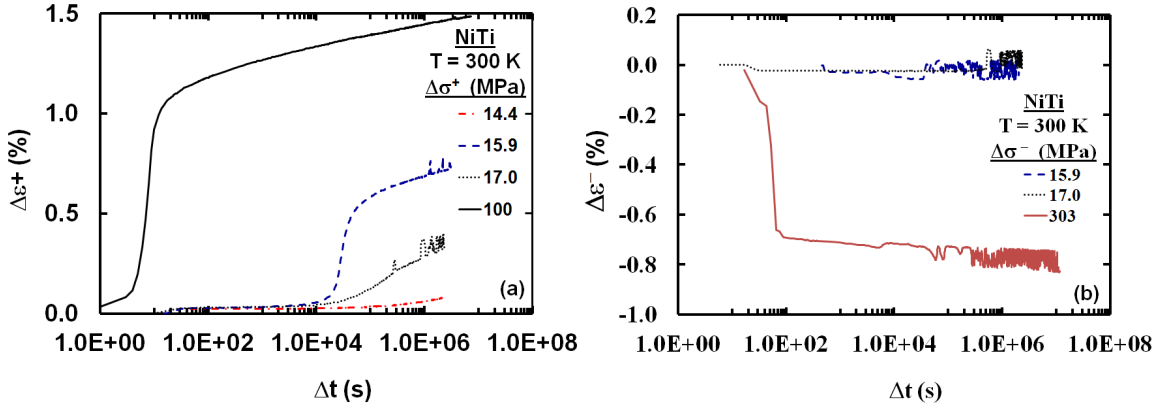

Figure 4.—The nature of the creep curves immediately after (a) a stress increase and (b) a stress decrease. The values of $\Delta\varepsilon$ and Δt are defined with respect to the point at which the stress change was performed. The + and – superscripts indicate increase and decrease, respectively. The curves for $\Delta\sigma^{+}$ = 14.4, 15.9 and 17.0 MPa do not start at Δt = 0 since the first data acquisition was acquired 10 s after the stress increase.

[1] The values of $\Delta\varepsilon$ and Δt are defined with respect to the point at which the stress change was performed. The + or – superscripts indicate increase or decrease, respectively. It is noted that the curves for $\Delta\sigma^{+}$ = 14.4, 15.9 and 17.0 MPa do not start at Δt = 0 since the first data acquisition was acquired 10 s after the stress increase.

A close examination of Figure 3(a) and Figure 4(a) reveals that although the magnitudes of the stress increases above 300 MPa were approximately similar varying between 14 and 17 MPa, the corresponding increases in $\Delta\varepsilon^{+}$ were not approximately equal. For example, $\Delta\varepsilon^{+}$ is much smaller when the stress is increased from 300 to about 314 MPa compared to that after a stress increase from about 314 to 330 MPa; the subsequent increase from about 330 to 347 MPa leads to an observed value of $\Delta\varepsilon^{+}$ somewhat intermediate (Figure 3(a) and Figure 4(a)). If the strain increase following the "incubation period" is attributed primarily to the reorientation and detwinning of the martensitic twin variants, then the present observations suggest that these mechanisms were sensitively dependent on the deformation microstructure present prior to the stress increase. In other words, there appears to be a close coupling between the deformation microstructure and the reorientation and detwinning of the martensitic twin variants at these low creep rates. Thus, it is suggested that the internal stress builds up during the "incubation period" as the alloy develops a dislocation microstructure as it creeps at a very low rate until the magnitude of this stress reaches a critical value when it triggers reorientation and detwinning of the martensitic twin variants.

Negligible amount of strain recovery was observed on stepwise unloading from 347.3 to 314.4 MPa, and unloading to a minimum stress of 11.4 MPa results in an instantaneous strain recovery of 0.66 percent and a total recovered strain of 0.82 percent after 3209.1 h following the stress decrease (Figure 4(b)). On decreasing the stress, $\Delta\varepsilon^{-}$ decreases slightly before becoming essentially constant when $\Delta\sigma^{-} \leq 17$ MPa. A large stress change of $\Delta\sigma^{-} = 303$ MPa, resulted in a large decrease in $\Delta\varepsilon^{-}$ followed by a continuing almost linear decrease in $\Delta\varepsilon^{-}$ with increasing Δt. This observation of anelastic creep can be attributed to the back flow of dislocations after the removal of the applied stress as the material attempts to reduce the internal back stress accumulated during deformation. Using an experimentally determined value of dynamic Young's modulus, E, of 72.2 GPa (Ref. 17), this recovered strain is close to the calculated elastic strain of 0.43 percent. Thus, a significant amount of residual strain of about 2.4 percent was measured in the specimen after testing for about 15 months (Figure 3(a)).

At 473 K corresponding to the austenitic phase, no measurable creep was observed below 220 MPa for creep times less than 1500 h but the creep strain increases dramatically above 220 MPa as the stress is increased by 23 MPa from 220 to 243 MPa (Figure 3(b)). However, the increases in creep strain were relatively small with subsequent increases in the applied stress varying between 24 and 38 MPa at each stress increase. The specimen continued to creep for several months at stresses exceeding 220 MPa. The observation of a very large increase in strain for a relatively small increase in stress from 220 to 243 MPa is interesting. This large increase in loading strain can be attributed to one or more factors: Dislocation nucleation and glide, stress-induced martensitic (SIM) transformation (Refs. 18, 19, 20, and 21) and deformation twinning of the B2 austenite (Refs. 20, 22, 23, 24, 25, 26, 27, and 28). Indeed, recent microstructural observations on a Ti-49.52 (at.%) Ni alloy crept at 773 K for 10 h and 0.75 h under stresses of 100 and 200 MPa, respectively, showed large amounts of deformation twins, "structural defects" at the interfaces of the twin plates and retained austenite in specimens furnace cooled to room temperature (Ref. 14). Interestingly, deformation twins were observed after a creep strain of 3 percent in a specimen crept at 773 K under a stress of 100 MPa corresponding to primary creep.

Based on the observations shown in Figure 3(a) and (b), it is reasonable to conclude that NiTi is unlikely to exhibit significant isothermal creep below 200 MPa between 300 and 473 K for creep times less than 2000 and 1500 h, respectively. Since the estimated creep rates are comparable to the resolution limits of the equipment ($\sim 10^{-10}$ s^{-1}), it is cautioned that measurable creep may occur in tests lasting several months or years.

3.3 Creep Characteristics of Martensitic NiTi at 300 K

Figure 5(a) and (b) show the ε–t plots for NiTi deformed at 300 K under an initial applied stress of 300 MPa corresponding to the martensitic phase. A very large strain increase of 2.6 percent was observed on loading followed by normal primary creep, where the creep rate rapidly decreases to values of about 7×10^{-10} s^{-1} (Figure 5(c)). For comparison, the estimated elastic strain at this value of applied stress is 0.42 percent using an experimental value of E = 72.2 GPa (Ref. 17). As will be demonstrated later, this additional contribution to the loading strain arises due to the reorientation and detwinning of the

martensitic twin variants. It is important to note that the specimen continued to creep very slowly over several months, where the creep strain increased to 2.8 percent after 3168 h. The data in Figure 5(a) was well-represented by Garofalo's logarithmic formulation (Ref. 29) so that $(\varepsilon_M)_{creep}$ (percent) = 3.0×10^{-2}log $(1+7.2\times10^{86}t)$, where t is in seconds. The coefficient of determination, R_d^2, was observed to be 0.992.

Figure 6(a) shows the creep curve for a NiTi specimen tested at 300 K under an initial applied stress of 350 MPa. The stress on the specimen was reduced to 5.2 MPa after it had crept for 2182 h and held at this lower stress for 1031 h before increasing the stress to 350 MPa. The stress was reduced once again to 5.2 MPa after 984.5 h, and the specimen was held at the lower stress for 676.2 h before increasing the stress to 350 MPa. The amount of decrease or increase in strain with each stress change varied between 0.62 and 0.67 percent. These values are 30 to 40 percent higher than the elastic strain, $(\varepsilon)_{elastic} \approx 0.48$ percent determined from the ratio, $\Delta\sigma/E$. A small amount of anelastic creep was observed after the stress decrease, where the strain continued to decrease with increasing time at a very low rate[2] for the entire time that the specimen was under 5.2. MPa (Figure 6(b)). On increasing the stress to 350 MPa, the creep strain increases rapidly to the value prior to the stress decrease without any overshoot unlike observations in pure metals. The observations of primary and anelastic creep lasting several thousand hours are indicative of dislocation activity. It is reasonable to conclude that dislocation glide-controlled creep is dominant in the martensitic phase at 300 K although its contribution to the total strain is quite small compared to the observed strain on loading.

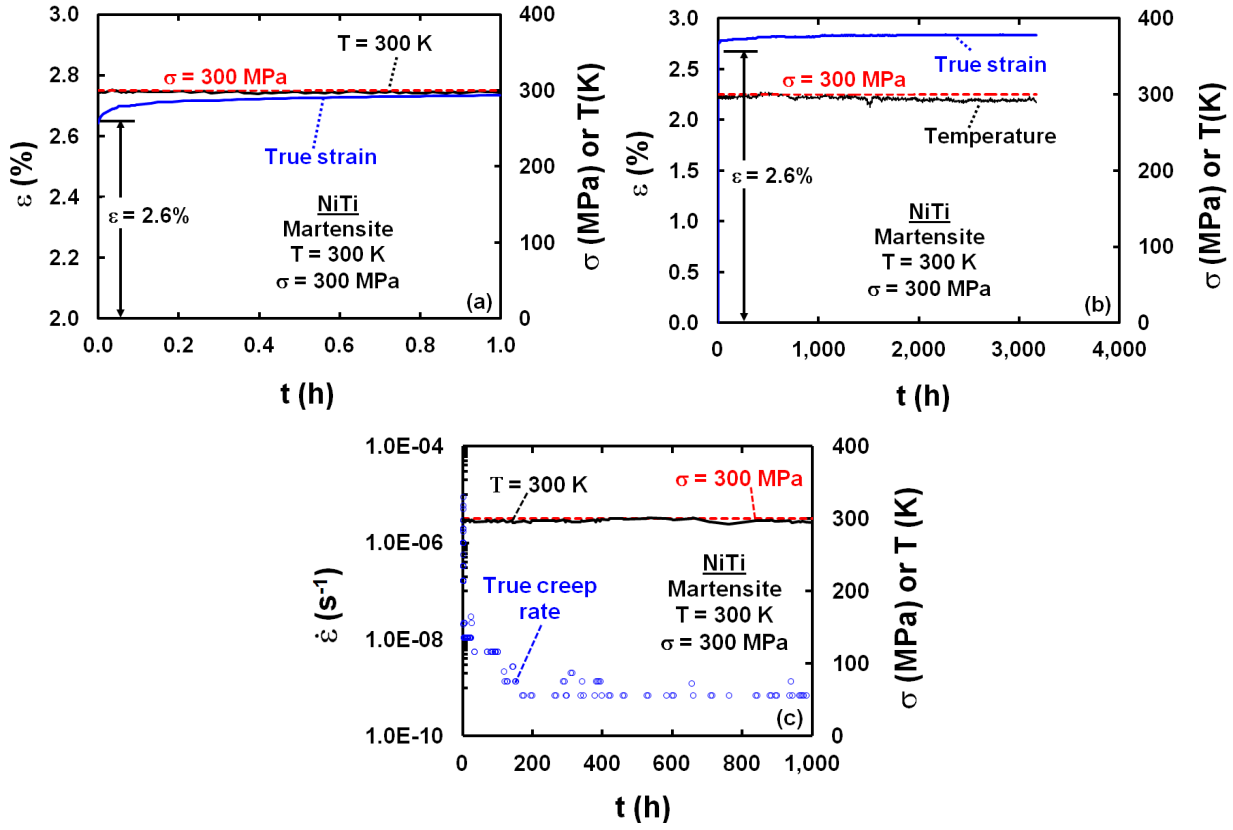

Figure 5.—Creep behavior of martensite at 300 K under an initial applied stress of 300 MPa. (a) Shape of the creep curve showing normal primary creep during the first hour after loading; (b) the full creep curve; (c) creep rate, $\dot{\varepsilon}$, versus time, t, plot.

[2] It is cautioned that the asymptotic nature of the creep curve shown in Figure 6(b) after the stress decrease may be due to the result of the creep rates approaching the resolution limits of the strain measurement system.

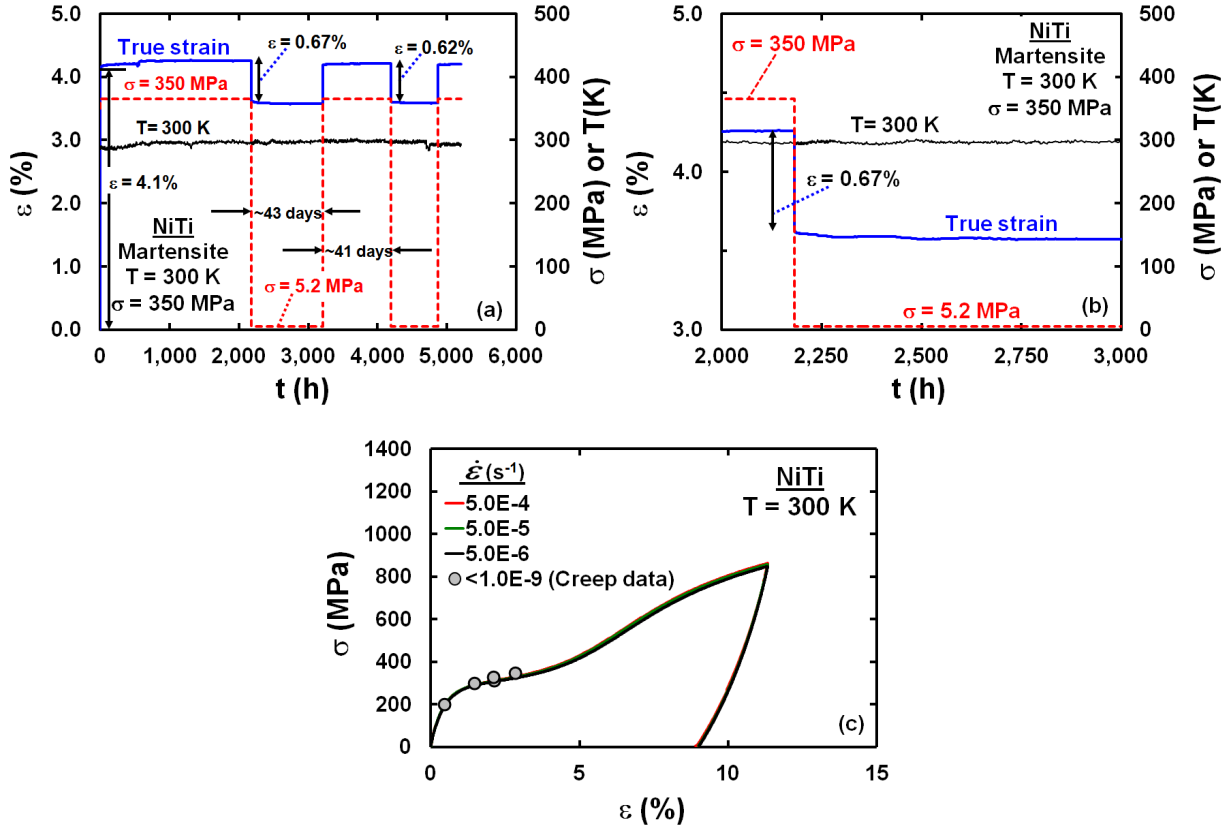

Figure 6.—Effect of stress changes on the creep behavior of NiTi at 300 K under an initial applied stress of 350 MPa. (a) Full creep curve; (b) magnified view of the creep curve after a stress decrease from 350 to 5.2 MPa showing anelastic creep; and (c) comparison of the creep data with the room temperature stress-strain curves for NiTi deformed under constant engineering strain rates varying between 5.0×10^{-6} and 5.0×10^{-4} s^{-1}. The creep data represent the measured values of the creep strain observed at the new value of the applied stress after the stress increase.

It is evident from Figure 5(a) and Figure 6(a) that a substantial contribution to the total creep strain is from the initial strain observed on first loading the specimen. In order to verify if this relatively large loading strain is due to the reorientation and detwinning of favorably oriented martensitic twins, the magnitudes of the loading strain after a stress increase at 300 K were superimposed on the room temperature stress-strain curve for NiTi (Ref. 30). The present data are in excellent agreement with the "plateau region" of the conventional stress-strain curve (Figure 6(c)). Importantly, these observations are independent of the strain rate. This region is attributed to the reorientation and detwinning of favorably oriented martensite twins (Ref. 18 and 31). The plateau in the tensile stress-strain curves have been attributed to "domino detwinning", where favorably-oriented martensitic twins detwin when the resolved stress reaches a critical value (Ref. 31). Such a process would require the existence of an "incubation period", where the creep strain is either negligible or low before a sudden increase in creep strain with increasing time. Figure 4(a) is consistent with this expected behavior.

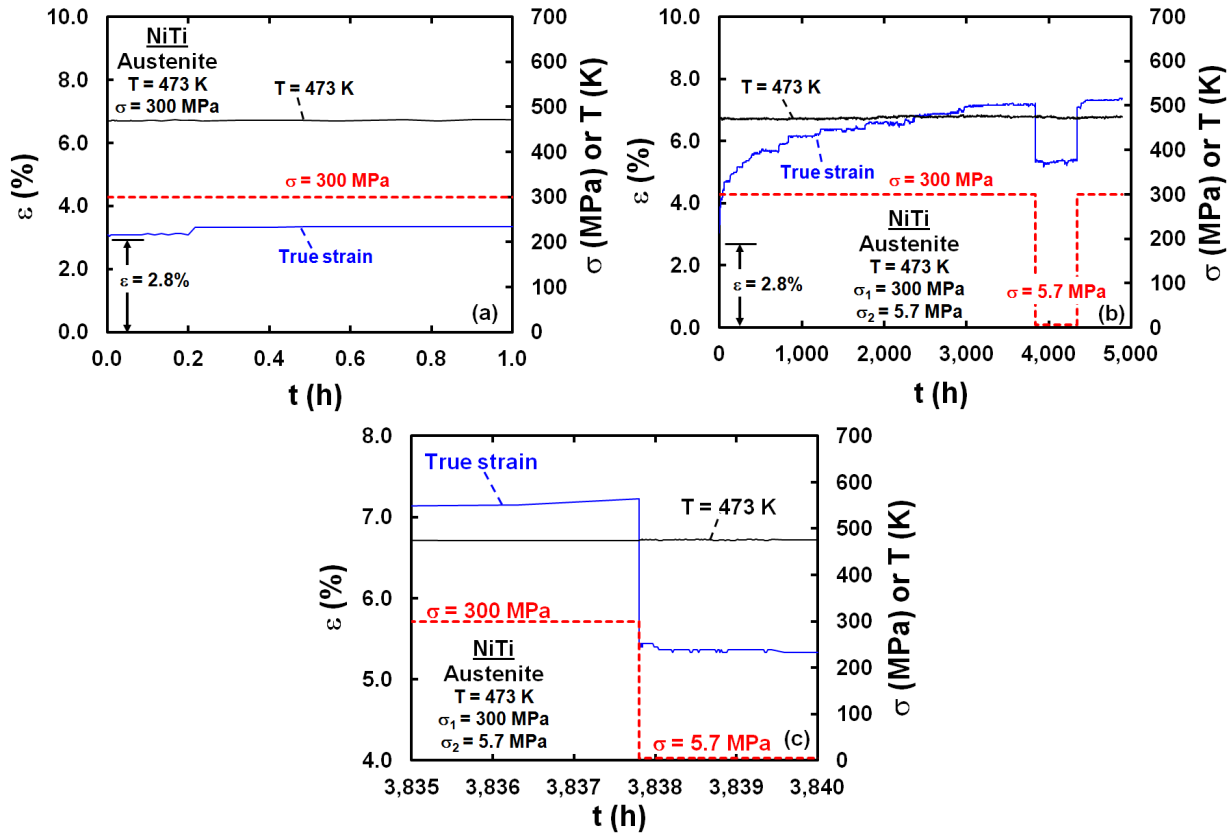

Figure 7.—Creep curves for NiTi deformed at 473 K under an initial applied stress of 300 MPa. (a) Initial portion of the creep curve within the first 1 h; (b) entire creep curve showing the effects of stress changes; and (c) magnified view of the creep curve after a stress decrease from 300 to 5.7 MPa showing anelastic creep.

3.4 Creep Characteristics of Austenitic NiTi at 473 K

Figure 7(a) to (c) show the creep curves for the austenitic phase at 473 K under an initial applied stress of 300 MPa. The loading strain is 2.8 percent, which is similar to that observed for the martensitic phase (Figure 5(a)). The estimated value of $(\varepsilon)_{elastic} \approx 0.35$ percent, where E = 87.1 GPa (Ref. 17). Significant normal primary creep characteristic of pure metal behavior was observed, where the creep strain increased to 7.2 percent in 3838 h (Figure 7(b)). Since austenitic NiTi has a B2 crystal structure with only three slip systems, the observation of this large creep strain can attributed to contributions from dislocation glide, stress-induced martensitic transformation and deformation twinning of the B2 austenite. There is a considerable body of experimental and theoretical evidence in support of deformation twinning in B2 NiTi and its alloys (Refs. 20, 22, 23, 24, 25, 26, 27, and 28). Recently, Ahadi and Rezaei (Ref. 14) reported the observation of large amounts of deformation twins in Ti-49.52 (at.%)Ni specimens crept at 773 K under a stress of 100 MPa for 10 h to a primary creep strain of 3 percent. These observations are consistent with the present results. On decreasing the stress to 5.7 MPa, the creep strain decreased to 5.4 percent, where this recovered strain, $(\varepsilon)_{recovery} \approx 6(\varepsilon)_{elastic}$. The strain continued to decrease with increasing time for as long as 502.3 h (~21 days) thereby indicative of the formation of a dislocation substructure in the alloy (Figure 7(b) and (c)). On increasing the stress back to 300 MPa, there is in an immediate increase in creep strain to 6.4 percent followed by a gradual increase to 7.4 percent after 549.3 h. Normal creep was observed after the stress increase characteristic of a dislocation glide-controlled process. The fact that the creep curve did not overshoot after the stress increase unlike observations in pure metals suggests that new dislocation sources were not significantly activated. Since

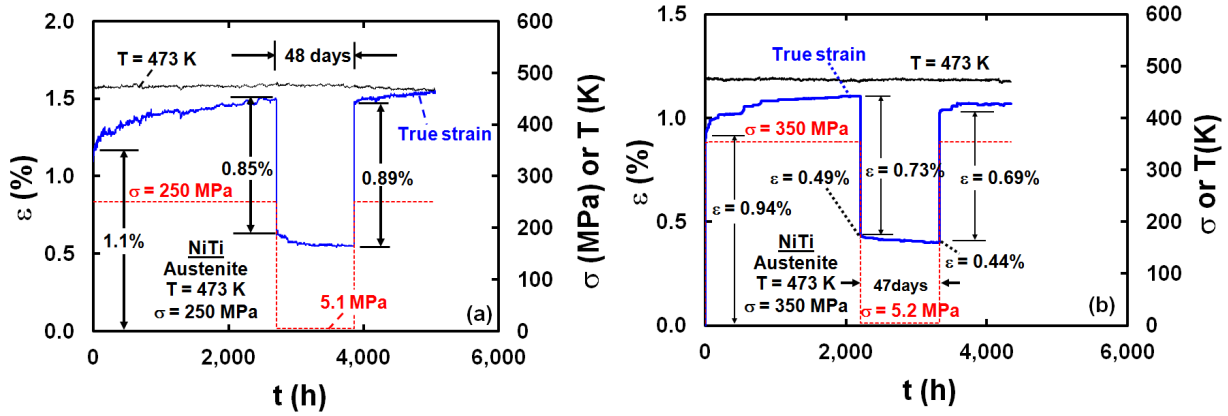

Figure 8.—Creep curves for NiTi crept at 473 K under an initial applied stress of (a) 250 and (b) 350 MPa showing the effect of stress changes and the existence of anelastic creep after a stress decrease.

the $(\varepsilon)_{recovery} \gg (\varepsilon)_{elastic}$, it is reasonable to assume that the austenite undergoes a stress-induced martensitic transformation on increasing the stress on the specimen (Refs. 18, 19, 20, and 21), and possibly during subsequent creep. In this case, the results from the stress decrease experiments suggest that $(\varepsilon)_{SIM} \approx 5(\varepsilon)_{elastic}$, where $(\varepsilon)_{SIM}$ is the strain due to stress-induced martensitic transformation.

Normal primary creep was also observed under an initial applied stress of 250 MPa with the measured instantaneous creep strain being 1.1 percent (Figure 8(a)). On decreasing the stress to 5.1 MPa, the creep strain decreased by 0.85 percent so that $(\varepsilon)_{recovery} \approx 3(\varepsilon)_{elastic}$. In this case, measurable anelastic creep was observed lasting for 1152.2 h (~48 days) prior to increasing the stress to 250 MPa. Once again, normal primary creep is observed after the stress increase. Since $(\varepsilon)_{recovery} \approx 3(\varepsilon)_{elastic}$, it is reasonable to assume that that $(\varepsilon)_{SIM} \approx 2(\varepsilon)_{elastic}$ since the amount of anelastic strain is much smaller (~0.04 percent). Figure 8(b) shows the creep results for NiTi deformed at 473 K under an initial applied stress of 350 MPa. Once again, anelastic creep lasting for over 47 days is observed on decreasing the stress from 350 to 5.2 MPa. The magnitude of $(\varepsilon)_{recovery} \approx 2(\varepsilon)_{elastic}$, so that $(\varepsilon)_{SIM} \approx (\varepsilon)_{elastic}$. Based on the observations shown in Figure 7 and Figure 8, it is clear that $(\varepsilon)_{elastic} \leq (\varepsilon)_{SIM} \leq 5(\varepsilon)_{elastic}$ with no consistent variation with increasing applied stress.

3.5 Creep Characteristics of Two-Phase NiTi at 373 K

Figure 9(a) to (c) show the creep curves for NiTi at 373 K under an initial applied stress of 300 MPa for various time intervals. The strain after loading was about 0.8 percent followed by normal primary creep, where the estimated creep rate was about 3×10^{-6} s^{-1} (Figure 9(a)). After about 1200 s into the test, the strain increased rapidly from about 1.8 to 5.0 percent within 1200 s. Normal primary creep was observed after this strain increase at an estimated creep rate of about 2×10^{-8} s^{-1}. A second rapid increase in strain was observed after a total creep time of 23.7 h, where the strain increased from about 5.4 to 6.6 percent in 1 h (Figure 9(b)). Once again, normal creep was observed after this strain increase lasting several thousand hours without any further rapid increase in creep strain and the specimen continued to creep to a strain of about 7.4 percent after 3192.1 h at which point the test was stopped (Figure 9(c)). The sudden increase in strain during creep suggests microstructural instability presumably due to stress-induced martensitic transformation. Alternatively, any delayed detwinning of any martensite present in the microstructure after an "incubation period" (Figure 4(a)) can also result in a large increase in strain.

Under an initial applied stress of 250 MPa, the loading strain was observed to be 1.4 percent (Figure 10), which is surprisingly twice as large as that observed under a creep stress of 300 MPa (Figure 9(a)). Normal primary creep was observed thereafter, where the creep strain increased to about 1.7 percent after about 2275 h. On reducing the stress to 5.4 MPa, the measured $(\varepsilon)_{recovery} \approx 1.3$ percent $\approx 4(\varepsilon)_{elastic}$ was

close to the value of the instantaneous creep strain. This large recovery in the creep strain suggests that the sudden increase in the creep strain observed at 300 MPa (Figure 9(a) and (b)) is likely due to a SIM transformation. Thus, $(\varepsilon)_{SIM} \approx 3(\varepsilon)_{elastic}$ at 373 K under an applied engineering stress of 250 MPa. In contrast to observations on austenite (Figure 8), the observed anelastic creep strain was quite small. This is similar to the behavior of the martensitic phase (Figure 6).

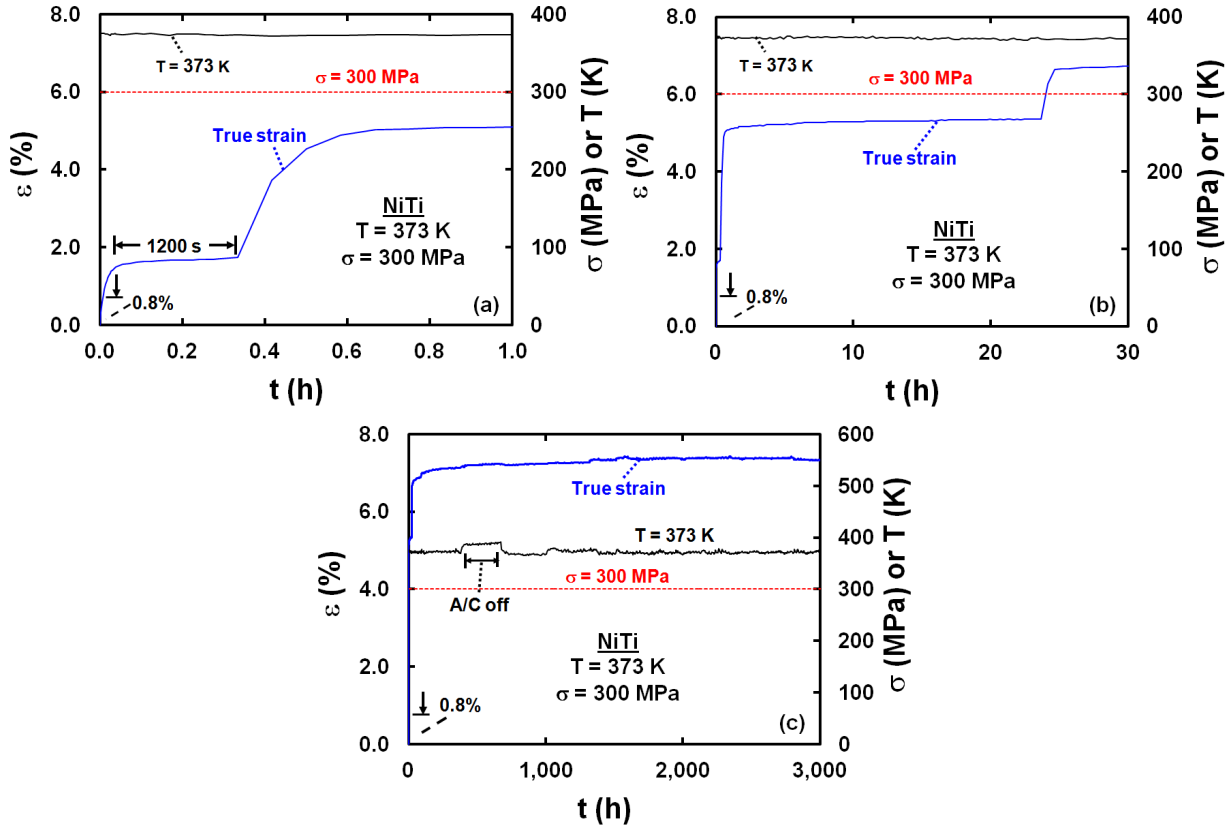

Figure 9.—Creep behavior of NiTi deformed at 373 K under an initial applied stress of 300 MPa. (a) and (b) show the relatively large increases in creep strain during the early stages of the test due to stress induced martensitic transformation, while (c) shows the entire creep curve.

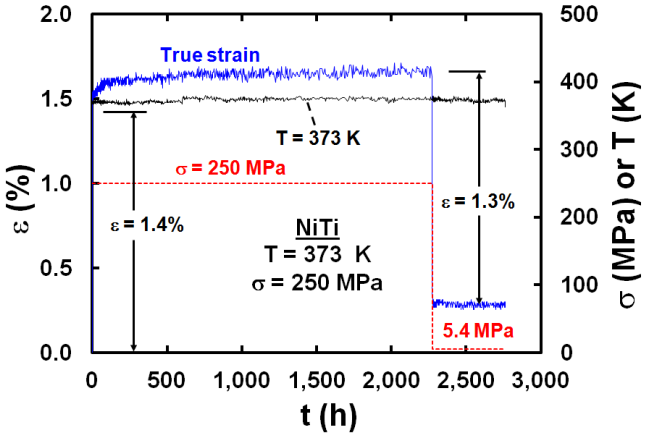

Figure 10.—Creep curve for NiTi deformed at 373 K under an initial applied stress of 250 MPa showing the effect of a stress reduction from 250 to 5.4 MPa.

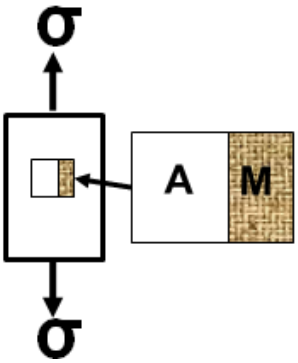

Figure 11.—Schematic showing the application of the Kelvin-Voigt model to adjacent austenitic (A) and martensitic (M) grains.

3.6 Strain Contributions

The present observations can be rationalized in a simple way using the Kelvin-Voigt model (Figure 11). Figure 11 shows the idealized duplex austenitic and martensitic microstructures arranged to satisfy the Kelvin-Voigt model. In this case, the strain is identical in both phases and the stresses are partitioned between the two phases as:

$$\varepsilon_T = \varepsilon_A = \varepsilon_M \tag{1a}$$

$$\sigma_T = V_A\sigma_A + \sum_1^n \left(V_M\sigma_M\right) \tag{1b}$$

where ε_T, ε_A and ε_M are the total creep strain, and the strains in the austenitic and martensitic phases, respectively, σ_T, σ_A and σ_M are the applied stress, and the effective stresses in the austenitic and n-variants of the martensitic phases, respectively, and V_A and V_M are the volume fractions of the austenitic and martensitic phase, respectively. Based on the observations shown in Figure 5 to Figure 10, we can write

$$\varepsilon_A = (\varepsilon_A)_{recovery} + (\varepsilon_A)_{anelastic} + (\varepsilon_A)_{creep} + (\varepsilon_A)_{twin} \tag{2a}$$

$$\varepsilon_M = (\varepsilon_M)_{recovery} + (\varepsilon_M)_{anelastic} + (\varepsilon_M)_{detwin} + (\varepsilon_M)_{creep} \tag{2b}$$

where $(\varepsilon_A)_{recovery}$ and $(\varepsilon_M)_{recovery}$ are the magnitudes of the recovered strain in the austenitic and martensitic phases, respectively, when the stress is decreased, $(\varepsilon_A)_{anelastic}$ and $(\varepsilon_M)_{anelastic}$ are the anelastic creep strains in the austenitic and martensitic phases, respectively, $(\varepsilon_A)_{creep}$ and $(\varepsilon_M)_{creep}$ are the plastic creep strains in the austenitic and martensitic phases, respectively, $(\varepsilon_A)_{twin}$ is the strain contribution from deformation twinning in the austenitic phase, and $(\varepsilon_M)_{detwin}$ is the strain due to the reorientation and detwinning of the martensitic phase. Since the measured recovery strain in the martensitic phase is within the measurement error of $(\varepsilon)_{elastic}$ (Fig. 6 (a)), it is reasonable to assume that $(\varepsilon_M)_{recovery} \approx (\varepsilon)_{elastic}$. In contrast, $(\varepsilon_A)_{recovery} \approx (\varepsilon_A)_{SIM} + (\varepsilon)_{elastic} \approx 2$ to $6(\varepsilon)_{elastic}$ for the creep of the austenitic phase (Figure 7, Figure 8 and Figure 10). The contributions of $(\varepsilon_A)_{anelastic}$ and $(\varepsilon_M)_{anelastic}$ to the total creep strain are small (Figure 6 to Figure 10) , so that, for simplicity, they can be neglected from Equations (2a) and (2b). The creep strain in the martensite due to dislocation glide is given by $(\varepsilon_M)_{creep} = (\alpha_M b_M)\int(\rho_M v_M)dt$, where α_M is a constant, b_M is the Burgers vector of the martensite, ρ_M is the dislocation density in the martensitic phase, and v_M is the dislocation

velocity in the martensite. The dislocation glide in the martensite is given by $v_M \propto \exp(B_M\sigma_M/RT)$, where B_M is a constant and R is the universal gas constant.

However, it is important to note that the observations of measurable anelastic creep in NiTi especially in the austenitic phase suggests that back stresses develop during creep in the material. Additionally, the observation of primary creep in the austenitic regime (Figure 2, Figure 4, Figure 7 and Figure 8) suggests a significant increase in the dislocation density so that a generalized representation of the creep strain is provided by $(\varepsilon_A)_{creep} = (\alpha AbA)\int(\rho_A v_A)dt$, where α_A is a constant, b_A is the Burgers vector of the austenite, ρ_A is the dislocation density in the austenitic phase, and v_A is the dislocation velocity in the austenite. The lack of steady-state creep suggests that the rate of dislocation hardening is greater than the rate of softening. Dislocation climb is not expected to be significant at 473 K, so that the dominant dislocation creep mechanisms are expected to be obstacle-controlled dislocation glide and/or dislocation cross-slip mechanisms (Ref. 32). Both these mechanisms predict a stress-dependent activation energy so that $v_A \propto \exp(B_A\sigma_A/RT)$, where B_A is a constant. However, contributions from the nucleation and growth of deformation twins to $(\varepsilon_A)_{creep}$ are also likely to be important as indicated in Equation (2a). The precise mechanistic contribution of deformation twinning to the creep of NiTi at 473 K is unclear.

3.7 Effect of Dislocation Activity on the Detwinning of the Martensite Twin Variants

The observation of sigmoidal creep behavior in the martensitic phase is significant since it suggests that detwinning of the martensitic twin variants is not instantaneous (Figure 4(a)). Following an "incubation period" consisting of a relatively insignificant increase in creep strain with increasing time, the subsequent sharp increase in the creep strain appears to be due to the reorientation and detwinning of the favorably oriented martensitic variants. However, the continued increase in creep strain after the strain rise with increasing time for as much as 2000 h suggests that most of the strain contribution is due to dislocation activity. A decrease in stress by 303 MPa results in an initial decrease in $\Delta\varepsilon \approx 0.7$ percent followed by a more gradual decrease in $\Delta\varepsilon$ with increasing time at an approximate creep rate of 1.5×10^{-10} s^{-1}, where the elastic strain recovery is expected to be about 0.43 percent for $\Delta\sigma = 300$ MPa similar to the experimental observations (Figure 4(b)). As noted earlier, a substantial amount of strain equal to about 2.4 percent was not recovered (Figure 1), which can be attributed to the detwinning of the martensitic variants as established by a comparison to the stress-strain behavior (Figure 6(c)).

The additional gradual time-dependent decrease in $\Delta\varepsilon$ (Figure 4(b)) is similar to anelastic creep observed in pure metals, where the observation of anelastic creep after a decrease in stress was attributed to the development of long-range internal back stresses due to the formation of a dislocation substructure during creep (Ref. 33). In pure metals and class M solid solution alloys, the observed magnitudes of anelastic strains are much larger than those reported in the present investigation due to the fact that these materials easily form heterogeneous cell and subgrain dislocation substructures, which result in the development of large internal back stresses in the material (Refs. 33 and 34). Hasegawa et al. (Ref. 34) observed sigmoidal creep in a Cu-16 (at. percent)Al solid solution alloy, where the creep rate first increased and then decreased as the total dislocation density increased with increasing creep time before saturating to a constant value beyond the peak creep rate. Correspondingly, the measured values of the long-range internal stress increased from about 30 percent to about 80 percent of the applied stress with increasing time as the dislocation substructure changed from isolated dislocations to dislocation cells as the creep time increased.

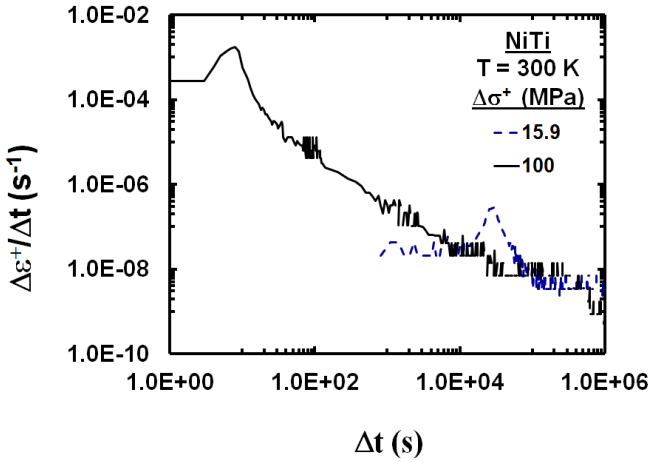

Figure 12.—Plot of $\Delta\varepsilon^+/\Delta t$ against Δt derived from Figure 4(a) for $\Delta\sigma^+$ values of 15.9 and 100 MPa showing the occurrence of peaks corresponding to the detwinning of the martensitic variants. The subsequent decrease in $\Delta\varepsilon^+/\Delta t$ with increasing Δt suggests a hardening of the creep curves due to an increase in the dislocation density.

Figure 12 shows that $\Delta\varepsilon^+/\Delta t$ first increases and then decreases with increasing Δt for $\Delta\sigma^+$ of 15.9 and 100 MPa; the magnitudes of $\Delta\varepsilon^+/\Delta t$ were determined from the time-dependent variation of the two well-defined sigmoidal curves shown in Figure 4(a). It is noted that these observations are valid for applied stresses exceeding 300 MPa (Figure 3(a)). The peak values of $\Delta\varepsilon^+/\Delta t$ were estimated to be 2.8×10^{-7} and 1.8×10^{-3} s^{-1} for 15.9 and 100 MPa, respectively. Significantly, there is a considerable decrease in the creep rate with increasing creep time after the occurrence of the maxima thereby indicating a hardening of the alloy due to the development of back stresses. Based on the observations of an "incubation period" in Figure 4(a) and anelastic creep in Figure 4(b), it is surmised that the detwinning of the martensitic variants is closely coupled with dislocation activity occurring within the twin plates or at the twin interfaces. The initial increase in $\Delta\varepsilon^+/\Delta t$ is primarily due to detwinning of the martensitic variants with some contributions from an increase in the dislocation density. The subsequent decrease in $\Delta\varepsilon^+/\Delta t$ after the peak values is mainly because of an increase in the long-range back stress due to the development of a dislocation substructure. These observations suggest that any attempt to model detwinning in this alloy must be coupled with a dislocation mechanism. Liu et al. (Ref. 35) observed a large number of dislocations networks at martensitic twin boundaries in NiTi deformed in tension. These observations are consistent with the present results.

3.8 Phenomenological Model for Detwinning

The phenomenological model shown in Figure 13 attempts to rationalize the role of dislocations on martensitic detwinning during low temperature creep of NiTi under tensile loading. Martensitic plates with twin variants, 1 and 2, meet at the twin boundary AB, where the open and solid circles represent the Ni and Ti atoms, respectively. It should be noted that boundaries, such as AB, have been termed as "habit plane variants" (hpv) while the interfaces within the twin variants have been referred to as "lattice correspondent variants" (lcv) (Ref. 36). Although the movement of hpv and lcv interfaces have been theoretically distinguished as "reorientation" and "detwinning" (Ref. 36), such specific distinctions could not be inferred from the present creep data. Thus, the movement of all twin boundary interfaces are collectively referred to as detwinning in this present paper.

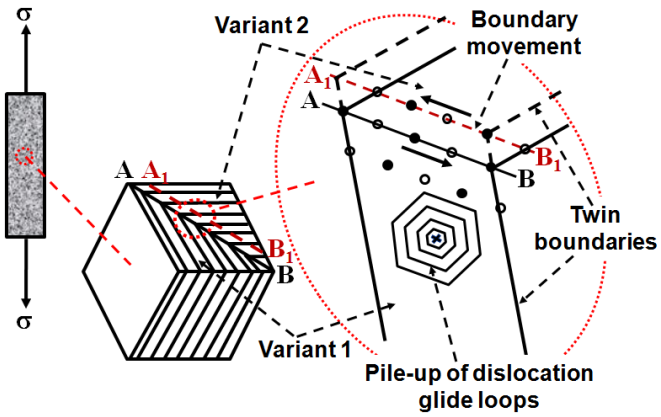

Figure 13.—Phenomenological model showing the possible role of dislocation pile-ups in martensitic variant 1, which results in the development of shear stresses in the boundary regions so that the boundary between variants 1 and 2 moves from AB to A_1B_1, and the corresponding detwinning of variant 2.

Dislocation loops emitted from sources within the martensitic twin variant 1 will expand under the action of the applied stress and pile-up at boundary AB so that a pile-up stress builds up on the lead dislocation at AB and in twin variant 2.[3] This stress build-up leads to a corresponding increase in the magnitudes of the shear stresses along AB and A_1B_1. When the magnitudes of the boundary shear stresses exceed a critical value, the pile-up loops will run into the boundary and it is anticipated that a shear wave will propagate in twin variant 2 due to instability brought about by a shuffling of the atoms from their present to their new positions along the shear direction, and a corresponding movement of the twin boundary from AB to A_1B_1 and beyond as the martensitic twin variant 2 undergoes detwinning. It is suggested that the observed "incubation time" (Figure 4(a)) is the time required for the build-up of the shear stresses along AB and A_1B_1. On the removal of the applied stress, any dislocation loops within variant 1 will contract thereby leading to anelastic creep. Alternatively, the shuffling of the atoms along A_1B_1 can involve short range diffusion in which case the process is likely to be thermally activated.

4.0 Summary and Conclusions

This paper presents the first published results on the effect of stress on the long term low temperature tensile creep behavior of nominally stoichiometric NiTi deformed at 300, 373 and 473 K under initial applied stresses between 200 and 350 MPa corresponding to the martensitic, two-phase and austenitic phase fields, respectively. The creep tests were conducted for several months to as long as 15 months. These observations revealed differences in the creep behavior of the two phases under constant stress and in stress change tests. The observed creep limit for the martensitic phase was determined to be 200 MPa at 300 K for creep times less than 2000 h. Similarly, the austenitic phase did not exhibit measurable creep below 220 MPa at 473 K for creep times less than 1500 h. However, it is cautioned that the validity of these creep limits is unknown for test times exceeding 2000 h and lasting several months or years since the estimated creep rates at 200 MPa were comparable to the resolution limits of the equipment ($\dot{\varepsilon} \sim 10^{-10}$ s^{-1}).

The martensitic phase exhibits a very large strain increase on loading followed by normal primary creep above 200 MPa. It is demonstrated that the magnitudes of the loading strains observed after stress increases coincide with the "plateau region" of the room temperature stress-strain curve for NiTi generated at constant strain rate. It is noted that the plateau is attributed to the reorientation and detwinning of favorable martensitic variants (Refs. 6, 18, 19, and 20). Significantly, sigmoidal creep is

[3] Alternatively, the dislocations can be emitted from the twin interfaces.

observed after a stress increase thereby suggesting the existence of an "incubation period" prior to the reorientation and the detwinning of the martensitic twins. A decrease in stress resulted in measurable anelastic creep lasting several thousand hours after an initial instantaneous strain decrease approximately equal to the elastic strain. The observation of normal primary creep and small amounts of anelastic creep is attributed to dislocation glide-controlled creep. A phenomenological dislocation creep model is proposed to rationalize the observations of an "incubation period" prior to detwinning of the twin variants in the martensite, where it is suggested that dislocation pile-up within one set of martensitic twin variants results in a build-up of shear stresses at its boundaries with other twin variants. Detwinning of the second twin variants occurs when the shear stresses exceed the critical stress required to cause the atoms to collectively shuffle to new positions thereby leading to the propagation of shear waves in these martensitic variants. The shuffling of these atoms can occur by short range diffusion.

Measurable creep was observed in the austenitic phase above 220 MPa at 473 K. Significant normal primary creep lasting several months was observed during the creep of the austenite. The relatively large creep strains observed in the B2 austenitic phase suggest that both dislocation glide and deformation twinning contribute to creep. The magnitudes of instantaneous creep strains after a stress decrease varied between 3 and $5(\varepsilon)_{elastic}$ depending on the value of the initial applied stress. It is suggested that a part of the austenitic creep strain is also due to stress-induced martensitic transformation of some of the austenite. Following a stress decrease, the creep strain continued to decrease for several days typical of anelastic creep and indicative of the formation of a dislocation substructure in the alloy. Normal primary creep was observed after a stress increase characteristic of a dislocation glide process. As expected, steady-state creep was not observed even after several months of testing. It is concluded that the creep of the austenitic phase occurs by a dislocation glide-controlled creep mechanism accommodated by the nucleation and growth of deformation twins. Normal primary creep was also observed at 373 K. However, sudden increases in the creep strain were observed within the first 1200 s after loading due to microstructural instability due to stress-induced martensitic transformation of the austenite present in the material.

References

1. J. Schweiger, in: M. Schwartz (Ed.), Encyclopedia of Smart Materials, John Wiley, New York, N. Y. vols. 1-2, 2002, pp. 42-59.
2. A. Chattopadhay, J. Rajadas: in: M. Schwartz (Ed.), Encyclopedia of Smart Materials, John Wiley, New York, N. Y. vols. 1-2, 2002, pp. 28-42.
3. T. A. Weisshaar, Multifunctional Structures/Integration of Sensors and Antennas, NATO Proceedings RTO-MP-AVT-141, Neuilly-sur-Seine, France, 2006, pp. O1-1 – O1-20, http://www.dtic.mil/cgi-bin/GetTRDoc?Location=U2&doc=GetTRDoc.pdf&AD=ADA479821.
4. F. T. Calkins, J. H. Mabe, G. W. Butler, in: Edward V. White (Ed.), Proc. SPIE Smart Structures and Materials 2006, vol. 6171, San Diego, CA, 2006, 61710O.
5. J. H. Mabe, F. T. Calkins, R. T. Ruggeri, in: Y. Matsuzaki, M. Ahmadian, D. J. Leo (Eds.), Proc. SPIE Smart Structures and Materials 2007, vol. 6525, San Diego, CA, 2007, 65251C.
6. J. Ma, I. Karaman and R. D. Noebe, Intern. Mater. Rev. 55 (2010) 257-315.
7. In: M. Schwartz (Ed.), Encyclopedia of Smart Materials, John Wiley, New York, N. Y. vols. 1-2, 2002.
8. A. K. Mukherjee, J. Appl. Phys. 19 (1968) 2201-2204.
9. H. Kato, T. Yamamoto, S. Hashimoto, S. Miura, Mater. Trans. JIM 40 (1999) 343-350.
10. E. Kobus, K. Neuking, G. Eggler, I. Wittkamp, Prakt. Metallogr. 39 (2002) 177-186.
11. G. Eggeler, J. Khalil-Allafi, K. Neuking, A. Dlouhý, Z. Metallkd. 93 (2002) 654-660.
12. C. Lexcelent, P. Robinet, J. Bernardini, D. L. Beke, P. Olier, Materialwiss. Werkstofftech, 36 (2005) 509-512.
13. S. M. Oppenheimer, A. R Yung, D. C. Dunand, Scripta Mater. 57 (2007) 377-380.
14. A. Ahadi, E. Rezaei, J. Mater. Eng. Perform. 21 (2012) 1806-1812.

15. A. Garg, unpublished research, Glenn Research Center, Cleveland, OH (2008).
16. S. Padula, S. Qiu, D. Gaydosh, R. Noebe, G. Bigelow, A. Garg, R. Vaidyanathan, Metal. Maters. Trans. 43A (2012) 4610-4621.
17. B. Lerch, unpublished research, NASA Glenn Research Center, Cleveland, OH (2009).
18. C. M. Wayman, T. W. Duerig, in: T. W. Duerig, K. N. Melton, D. Stöckel, C. M. Wayman (Eds.), Engineering Aspects of Shape Memory Alloys, Butterworth-Heinemann, London,1990, pp. 3-20.
19. C. M. Wayman, Prog. Mater. Sci. 36 (1992) 203-224.
20. K. Otsuka, X. Ren, Intermetall., 7 (1999) 511-528.
21. L. C. Brinson, I. Schmidt, R. Lammering, J. Mechan. Physics Solids 52 (2004) 1549-1571.
22. E. Goo, T. Duerig, K. Melton, R. Sinclair, Acta Metall. 33 (1985) 1725-1733.
23. E. Hornbogen, J. Mater. Sci. 34 (1999) 599-606.
24. S. Ii, K. Yamauchi, Y. Maruhashi and M. Nishida, Scripta Mater., 49 (2003) 723-727.
25. A.N. Tyumentsev, N.S. Surikova, I.Yu. Litovchenko, Yu.P. Pinzhin, A.D. Korotaev, O.V. Lysenko, Acta Mater. 52 (2004) 2067-2074.
26. M. Nishida, M. Matsuda, T. Fujimoto, K. Tanka, A. Kakisaka, H. Nakashima, Mater. Sci. Eng. A 438-440 (2006) 495-499.
27. T. Ezaz, H. Sehitoglu, Appl. Phys. Lett. 98 (2011) 241906-1-241906-3.
28. A. Ahadi, E. Rezaei, J. Mater. Eng. Perform., 21 (2012) 1806-1812.
29. F. Garofalo, Fundamentals of Creep and Creep-Rupture in Metals, Macmillan, New York, NY, 1966.
30. D. Gaydosh, S. Padula, unpublished research, Glenn Research Center, Cleveland, OH (2007).
31. Y. Liu, Proceedings of SPIE 4234 (2001) 82-92.
32. S. V. Raj, Mater. Sci. Eng. A 322 (2002) 132-147.
33. W. D. Nix, B. Illschner, in: P. Haasen, V. Gerold, G. Kostorz (Eds.), Strength of Metals and Alloys, vol. 3, Pergamon Press, Oxford, 1980, pp. 1503-1530.
34. T. Hasegawa, Y. Ikeuchi, S. Karashima, Metal Sci. J. 6 (1972) 78-82.
35. Y. Liu, Z. Xie, J. V. Humbeeck, L. Delaey, Acta Mater. 46 (1998) 4325-4338.
36. P. Thamburaja, J. Mech. Phys. Solids 53 (2005) 825-856.

REPORT DOCUMENTATION PAGE	Form Approved OMB No. 0704-0188

1. REPORT DATE *(DD-MM-YYYY)*	2. REPORT TYPE	3. DATES COVERED *(From - To)*
01-06-2013	Technical Memorandum	

4. TITLE AND SUBTITLE
Low Temperature Creep of Hot-Extruded Near-Stoichiometric NiTi Shape Memory Alloy
Part I: Isothermal Creep

5a. CONTRACT NUMBER

5b. GRANT NUMBER

5c. PROGRAM ELEMENT NUMBER

6. AUTHOR(S)
Raj, S., V.; Noebe, R., D.

5d. PROJECT NUMBER

5e. TASK NUMBER

5f. WORK UNIT NUMBER
WBS 561581.02.08.47.05.04

7. PERFORMING ORGANIZATION NAME(S) AND ADDRESS(ES)
National Aeronautics and Space Administration
John H. Glenn Research Center at Lewis Field
Cleveland, Ohio 44135-3191

8. PERFORMING ORGANIZATION REPORT NUMBER
E-18699-1

9. SPONSORING/MONITORING AGENCY NAME(S) AND ADDRESS(ES)
National Aeronautics and Space Administration
Washington, DC 20546-0001

10. SPONSORING/MONITOR'S ACRONYM(S)
NASA

11. SPONSORING/MONITORING REPORT NUMBER
NASA/TM-2013-217888-PART1

12. DISTRIBUTION/AVAILABILITY STATEMENT
Unclassified-Unlimited
Subject Category: 26
Available electronically at http://www.sti.nasa.gov
This publication is available from the NASA Center for AeroSpace Information, 443-757-5802

13. SUPPLEMENTARY NOTES
Submitted to Materials Science & Engineering A, Elsevier.

14. ABSTRACT
This two-part paper is the first published report on the long term, low temperature creep of hot-extruded near-stoichiometric NiTi. Constant load tensile creep tests were conducted on hot-extruded near-stoichiometric NiTi at 300, 373 and 473 K under initial applied stresses varying between 200 and 350 MPa as long as 15 months. These temperatures corresponded to the martensitic, two-phase and austenitic phase regions, respectively. Normal primary creep lasting several months was observed under all conditions indicating dislocation activity. Although steady-state creep was not observed under these conditions, the estimated creep rates varied between 10^{-10} and 10^{-9} s^{-1}. The creep behavior of the two phases showed significant differences. The martensitic phase exhibited a large strain on loading followed by a primary creep region accumulating a small amount of strain over a period of several months. The loading strain was attributed to the detwinning of the martensitic phase whereas the subsequent strain accumulation was attributed to dislocation glide-controlled creep. An “incubation period” was observed before the occurrence of detwinning. In contrast, the austenitic phase exhibited a relatively smaller loading strain followed by a primary creep region, where the creep strain continued to increase over several months. It is concluded that the creep of the austenitic phase occurs by a dislocation glide-controlled creep mechanism as well as by the nucleation and growth of deformation twins.

15. SUBJECT TERMS
Low temperature creep; NiTi; Shape memory alloys; intermetallic alloys

16. SECURITY CLASSIFICATION OF:			17. LIMITATION OF ABSTRACT	18. NUMBER OF PAGES	19a. NAME OF RESPONSIBLE PERSON
a. REPORT	b. ABSTRACT	c. THIS PAGE			STI Help Desk (email:help@sti.nasa.gov)
U	U	U	UU	24	19b. TELEPHONE NUMBER *(include area code)* 443-757-5802